Research Article | Vol. 31, No. 9 / 24 Apr 2023 / Optics Express 13566
Optics EXPRESS

Numerical analysis of the ultra-wide tunability of nanofiber Bragg cavities

HIDEAKI TAKASHIMA,[1] ANDREAS W. SCHELL,[2,3,4] AND SHIGEKI TAKEUCHI[1,*]

[1]Graduate School of Engineering, Kyoto University, Kyoto daigaku-Katsura, Nishikyo-ku, Kyoto 615-8530, Japan
[2]Institut für Festkörperphysik, Leibniz Universität Hannover, 30167 Hannover, Germany
[3]Physikalisch-Technische Bundesanstalt, 38116 Braunschweig, Germany
[4]Institute of Semiconductor and Solid State Physics, Johannes Kepler University, Linz 4040, Austria
*takeuchi@kuee.kyoto-u.ac.jp

Abstract: Nanofiber Bragg cavities (NFBCs) are solid-state microcavities fabricated in optical tapered fiber. They can be tuned to a resonance wavelength of more than 20 nm by applying mechanical tension. This property is important for matching the resonance wavelength of an NFBC with the emission wavelength of single-photon emitters. However, the mechanism of the ultra-wide tunability and the limitation of the tuning range have not yet been clarified. It is important to comprehensively analyze both the deformation of the cavity structure in an NFBC and the change in the optical properties due to the deformation. Here, we present an analysis of the ultra-wide tunability of an NFBC and the limitation of the tuning range using three dimensional (3D) finite element method (FEM) and 3D finite-difference time-domain (FDTD) optical simulations. When we applied a tensile force of 200 μN to the NFBC, a stress of 5.18 GPa was concentrated at the groove in the grating. The grating period was extended from 300 to 313.2 nm, while the diameter slightly shrank from 300 to 297.1 nm in the direction of the grooves and from 300 to 298 nm in the direction orthogonal to the grooves. This deformation shifted the resonance peak by 21.5 nm. These simulations indicated that both the elongation of the grating period and the small shrinkage of the diameter contributed to the ultra-wide tunability of the NFBC. We also calculated the dependence of the stress at the groove, the resonance wavelength, and the quality Q factor while changing the total elongation of the NFBC. The dependence of the stress on the elongation was 1.68×10^{-2} GPa/μm. The dependence of the resonance wavelength was 0.07 nm/μm, which almost agrees with the experimental result. When the NFBC, assumed to have the total length of 32 mm, was stretched by 380 μm with the tensile force of 250 μN, the Q factor for the polarization mode parallel to the groove changed from 535 to 443, which corresponded to a change in Purcell factor from 5.3 to 4.9. This slight reduction seems acceptable for the application as single photon sources. Furthermore, assuming a rupture strain of the nanofiber of 10 GPa, it was estimated that the resonance peak could be shifted by up to about 42 nm.

1. Introduction

Solid-state optical microcavities coupled with single-photon emitters have attracted attention in various applications such as optical sensors [1], microlasers [2], cavity optomechanics [3], and quantum information devices [4–8]. To realize these applications, it is important to match the resonance wavelength of the cavities with the emission wavelength of single-photon emitters. Conventional solid-state nano- and microcavities have realized resonance tuning using various methods, such as temperature control [9–11], laser-pumped thermal tuning [12,13], electrical thermo-optic tuning [14], gas condensation on the surface of the cavities [15,16], and mechanical

#483843 https://doi.org/10.1364/OE.483843
Journal © 2023 Received 21 Dec 2022; revised 17 Feb 2023; accepted 3 Mar 2023; published 11 Apr 2023

Optics EXPRESS

tuning [17]. However, the tuning range for conventional nano- and microcavities is typically less than 5 nm. Therefore, it is desirable to develop solid-state cavities with wider tuning ranges.

Nanofiber Bragg cavities (NFBCs), which consist of periodic grooves with a defect region on a nanofiber, have been developed recently as solid-state cavities with ultra-wide tunability [18–23]. An optical nanofiber is a single-mode optical fiber with a diameter corresponding to about half the free-space wavelength of the light used [24–32]. Photons emitted from single-photon emitters close to the surface of the nanofiber can be coupled to the nanofiber via a strong evanescent field with an efficiency of at most 30% [26,27]. To improve the coupling efficiency, nanofibers containing cavity structures have recently been developed [18–23,33,34]. The resonance wavelength of these cavities can be tuned by applying mechanical tension [19,33]. Nayak *et al.* realized a resonance-peak shift for a fiber-based photonic crystal cavity using a piezo actuator [33]. We have also achieved reversible and linear ultra-wide tuning of the resonance wavelength by over 20 nm [19]. However, the mechanism of the ultra-wide tunability of NFBCs has not been clarified in detail. To understand this mechanism, it is necessary to comprehensively determine both the deformation of the cavity structure and the change in the optical properties when mechanical tension is applied.

In this paper, we present the analysis of the mechanism of ultra-wide tunability of NFBCs and the limitation of the tuning range based on three dimensional (3D) finite element method (FEM) (COMSOL Multiphysics) and 3D finite-difference time-domain (FDTD) optical simulations (FDTD solutions, Lumerical). As the calculation model, we considered a NFBC geometry that consists of a nanofiber with periodic nano-grooves with a defect on one of the sides. When a tensile force of 200 μN was applied to the NFBC, a stress of 5.18 GPa was concentrated at the bottoms of the grooves in the grating. In addition, the grating period increased from 300 to 313.2 nm, while the diameter slightly shrank from 300 to 297.1 nm in the direction of the sides of the grooves and from 300 to 298 nm in the direction orthogonal to the sides of the grooves. At the same time, the resonance peak shifted from 634.4 to 655.9 nm. From this analysis, it is understood that the ultra-wide tunability of the NFBC is due to the increase of the grating period and the slight shrinking of the diameter. We also calculated the dependence of the stress at the groove, the resonance wavelength, and the quality (Q) factor while changing the total length of the NFBC. The dependence of the stress and the resonance wavelength on the NFBC length were 1.68×10^{-2} GPa/μm and 0.07 nm/μm, respectively. When the NFBC was stretched by 380 μm, the Q factor changed from 535 to 443, which corresponds to a change in the Purcell factor from 5.3 to 4.9. Furthermore, assuming a rupture strain for the nanofiber of 10 GPa, we estimated that the tuning range could be extended to about 42 nm.

This paper is organized as follows: Section 2 explains the calculation model and calculation procedure in this analysis. In section 3, we explain the calculation methods for the deformation of the NFBC and the optical properties. Section 4 shows the calculation results for the deformation of the NFBC and the resonance spectra as well as the dependence of the stress, peak shift, and the Q factors on the total lengthening of the NFBC. Finally, section 5 concludes the paper.

2. Calculation model and calculation procedure

Here, we consider the calculation model of an NFBC used in this analysis. Figure 1(a) shows the sketch of the model. We took an NFBC consisting of two parts: a taper waist, including a cavity part, and tapers. Note that thick tapers and pigtails of single mode fiber can be ignored since they have little effect on the elongation, as described later. The taper waist had a constant diameter of 300 nm, while the tapers became exponentially thicker towards their ends. A cavity was created at the center of the taper waist by increasing the distance between the two gratings. Figure 1(b) is a magnified view of the taper waist including the cavity. As an approximation for the calculations, we employed periodic nano-grooves on the sides of the nanofiber for the shape of the grating. The period of the grooves, the groove depth, and the total number of periods were set to 300 nm,

Optics EXPRESS

45 nm, and 160, respectively. The defect with a length of 450 nm is introduced in the middle of the grating according to the structure of the NFBC used in the former experiment [19].

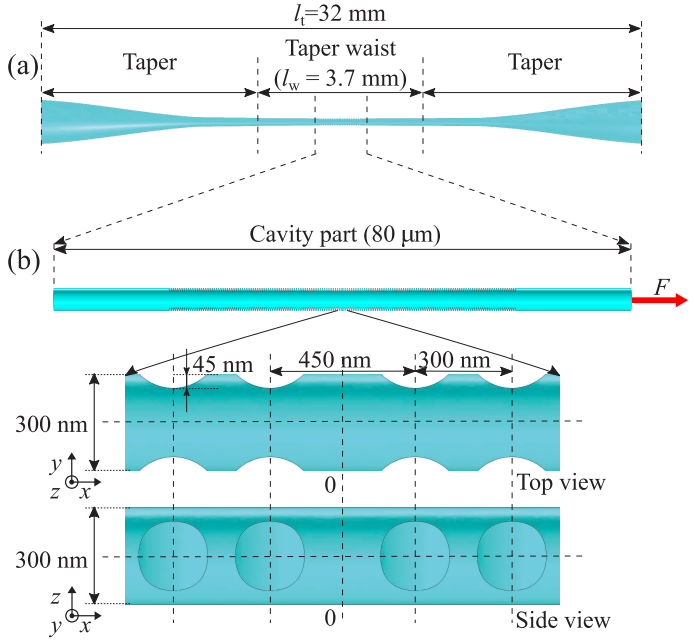

Fig. 1. (a) Sketch of calculation model. l_w is the length of the taper waist and l_t is the length of the calculation range. A cavity is created at the center of the taper waist. (b) Detailed view of the taper waist including cavity. The diameter of the taper waist is 300 nm. The period of the grooves, the groove depth, and the total number of periods are 300 nm, 45 nm, and 160, respectively. The defect at the center of the grating has a length of 450 nm. A tensile force F (a red arrow) is applied to one end of the cavity in the FEM simulations.

We consider the radial profile of the calculation model. The radial profile at any position x along the long axis of the model takes the following form [35],

$$r(x) = \begin{cases} r_w e^{-\chi(x+l_w/2)} & -l_t/2 \le x \le -l_w/2 \\ r_w & -l_w/2 \le x \le l_w/2 \\ r_w e^{\chi(x-l_w/2)} & l_w/2 \le x \le l_t/2. \end{cases} \quad (1)$$

Here, r_w is the radius of the taper waist, l_w is the length of the taper waist, l_t is the length of the calculation range, and the exponent χ has dimensions of inverse length. By fitting the radial profile for a fabricated nanofiber, obtained using a scanning electron microscopy (SEM), and setting l_t = 32 mm, r_w, l_w, and χ were determined to be 150 nm, 3.7 mm, and 0.238/mm, respectively.

Next, we describe the calculation procedure used in this analysis. First, the deformation at the center of the taper waist including the cavity (cavity part), shown in Fig. 1(b), was simulated using the solid mechanism module in COMSOL Multiphysics. Then, the calculated structures were imported into the 3D FDTD software as calculation models, and their optical properties were calculated. Finally, the dependence of the stress at the groove, the resonance wavelength, and the Q factor on the total elongation of the NFBC was calculated while changing the tensile force. Note that we used an FDTD simulation instead of an FEM simulation for calculation of the optical properties in order to reduce the computational time.

Optics EXPRESS

3. Calculation methods

3.1. Calculation method for cavity part

The solid mechanics module in COMSOL was used to calculate the deformation of the cavity structure in the NFBC. The length of the calculation model was set to 80 μm, corresponding to the center part of the taper waist including the cavity as shown in Fig. 1(b). In this analysis, we assumed a linear stress-strain relationship (Hooke's law), due to the fact that the resonance wavelength for the NFBC was linearly shifted in our reported experiment [19]. We used the material properties of SiO_2 with a density of 2203 kg/m^3, a Young's Modulus E of 73.1 GPa, and a Poisson ratio ν of 0.17. One end of the cavity part was fixed and a tensile force F was uniformly applied to the other end. We used a free tetrahedral mesh with a maximum element size of 50 nm and a minimum element size of 1 nm.

3.2. Calculation method for total elongation of NFBC

Here, we consider the total elongation Δl_t for the calculation model assuming a linear stress-strain relationship. Δl_t can be calculated from the sum of the elongation of the cavity part, calculated by the FEM, and the elongation of the nanofiber (NFBC excluding the cavity part) Δl_n. The stress-strain relationship at any position x along the long axis of the nanofiber can be written as [35]

$$\sigma(x) = E\epsilon(x), \tag{2}$$

where $\sigma(x)$ is the stress and $\epsilon(x)$ is the strain. $\sigma(x)$ can be defined as

$$\sigma(x) = \frac{F}{\pi r(x)^2}. \tag{3}$$

From Eqs. (2) and (3), $\epsilon(x)$ can be written as

$$\epsilon(x) = \frac{F}{\pi E r(x)^2}. \tag{4}$$

Δl_n can be expressed by integrating $\epsilon(x)$,

$$\Delta l_\mathrm{n} = \int_{-l_\mathrm{t}/2}^{l_\mathrm{t}/2} \epsilon(x)dx = \frac{F}{\pi E}\int_{-l_\mathrm{t}/2}^{l_\mathrm{t}/2} \frac{1}{r(x)^2}dx. \tag{5}$$

In this analysis, Δl_n was calculated assuming a length of the taper waist of 3.62 mm, which was the length of the taper waist minus the length of the cavity part. Note that the contribution of the thick parts, i.e., the thick tapers and the pigtails for the single-mode fiber, to the total elongation was negligibly small since the strain is inversely proportional to the square of the radius.

When a silica fiber with constant diameter d and length of l is stretched by a force F, it shrinks along its lateral direction. This lateral strain is proportional to the longitudinal strain ϵ in the elastic range. Hence, the change in diameter Δd is given by

$$\Delta d = -\nu\epsilon d. \tag{6}$$

3.3. Calculation method for optical properties

To calculate the optical properties, we performed 3D FDTD simulations [36]. For this calculation, the structures calculated by the FEM were imported into the FDTD software in the format of standard triangulated language (StL). The calculation area for the FDTD simulations was set to $60 \times 2 \times 2$ μm^3. To calculate resonance spectra, the light source was placed at a location -24 μm from the center of the simulation region and the transmission was monitored 28 μm from

Optics EXPRESS

the center of the simulation region. The polarization of the light source was set to y-polarized mode or z-polarized mode. We used an automatic non-uniform mesh. The Q factor is calculated from the resonance and the full width half maximum (FWHM) of the resonant peak in the FDTD simulation. The Purcell factor at the resonance wavelength when an electrical dipole was placed at the position where the intensity of the electric field was a maximum outside the nanofiber was calculated from P_{cav}/P_0, where P_{cav} is the power emitted by a dipole in the cavity and P_0 is the power radiated in the vacuum.

4. Results and discussion

In this section, we show the calculation results for the deformation of the NFBC and the resonance spectra. We also show the calculation results for the stress at the groove, the resonance-peak shift, and Q factors to the total elongation Δl_t.

4.1. Deformation of cavity structure

We present the results of the deformation of the NFBC obtained by the FEM simulation. Figure 2 shows the calculated stress with the deformed cavity parameters. An F of 200 μN was applied to one end of the cavity part. It can be seen that the stress is concentrated at the grooves, and is 5.18 GPa at position A. This is less than the rupture stress σ_{rup} for a silica nanowire with a diameter of 300 nm ($\sigma_{rup} > 10$ GPa) [37]. The stress is relieved outside the grooves (1.07 GPa at position B). Therefore, the NFBC with the etched grooves has an effect on the rupture stress. The pitch of the grooves (between positions A and C) increases from 300 to 313.2 nm. The change in diameter is slightly asymmetric for each axis. In the y-axis direction, the diameter shrunk from 300 to 297.1 nm, whereas in the z-axis direction, the diameter shrunk from 300 to 298 nm.

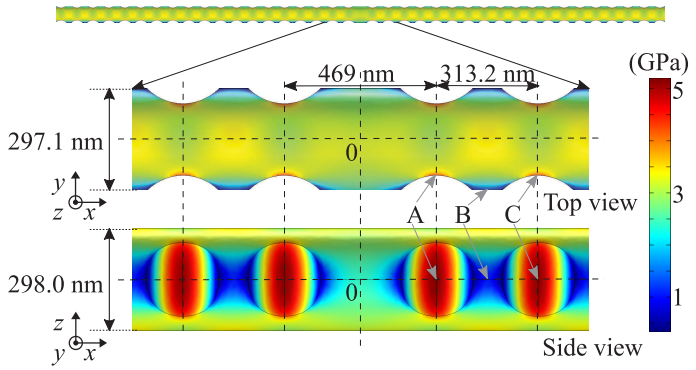

Fig. 2. Calculation results of FEM simulation.

To confirm the calculation results of the FEM, we compared them with an analysis of the deformation based on a simple model where the main deformation of the NFBC can be understood as a change in the shape of a silica cylinder with a diameter of 300 nm. When the cylinder was stretched by a force F of 200 μN, the stress was calculated to be 2.83 GPa from Eq. (3). From Eq. (5), the grating period increased from 300 to 311.6 nm, while the diameter decreased from 300 to 298 nm from Eq. (6). As expected, these results are slightly smaller than the calculation results of the FEM. This is because the simple model did not take into account the effect of the grooves. Based on this reasonable agreement, we performed the following calculations using the cavity structures analyzed by the FEM.

Optics EXPRESS

4.2. Calculation results for resonance spectra

We calculated the resonance spectra when $F = 200$ μN was applied to the cavity part of the NFBC. Figure 3(a) and (b) show the results of the FDTD simulations for y-polarized mode and z-polarized mode, respectively, when the cavity structures simulated by the FEM were used for the FDTD calculation model. Before stretching the NFBC, a resonance peak appeared at a wavelength of 634.4 nm (black solid line) for the y-polarized mode. This peak shifted to 655.9 nm under the tensile force (black dotted line). On the other hand, a resonance peak for the z-polarized mode shifted from 638.2 nm to 659.5 nm. We also calculated the changes in the effective refractive indices for y-polarized mode at the center of the cavity region and the bottom of a groove using the FDTD method. They were slightly reduced from 1.0724 to 1.0604 and 1.0367 to 1.0287, respectively, due to the change in the structure caused by the tensile force. These reductions slightly reduced the resonance wavelength. Therefore, we found that elongation of the grating period greatly contributes to the ultra-wide tunability of the NFBC.

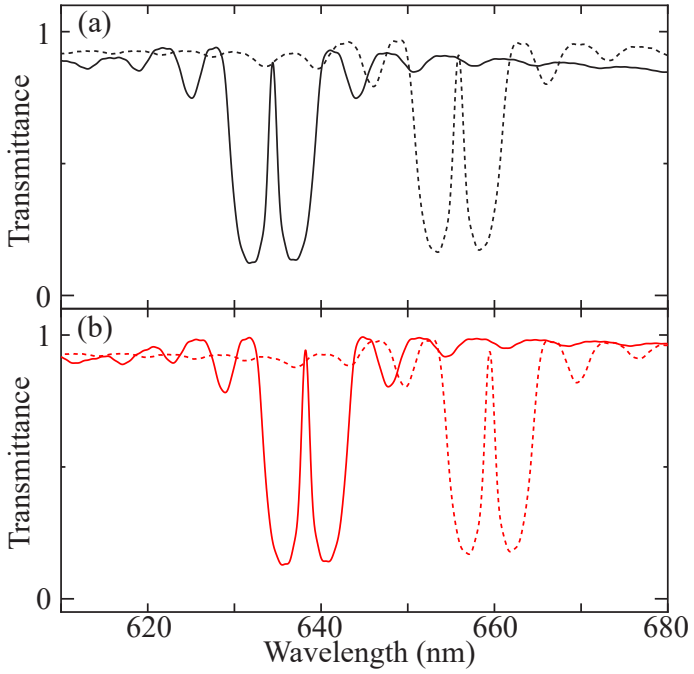

Fig. 3. Calculated resonance spectra from FEM simulation for (a) y-polarized mode and (b) z-polarized mode. The solid line and dotted line are $F = 0$ and $F = 200$ μN, respectively.

4.3. Dependence of stress, resonance peak, and Q factor on total elongation of NFBC

We calculated the total elongation Δl_t while changing F. Figure 4(a) shows the calculation results. The black dots are the calculation results and the dotted line indicates the results of fitting using a linear function. The NFBC was stretched with a tensile force rate of 1.55 μm/μN. We then calculated the dependence of the stress at the groove (position A in Fig. 2) based on this calculated total elongation Δl_t. Figure 4(b) shows the calculation results. The black squares are the calculation results and the short chained line indicates the result of fitting using a liner function. The stress increased linearly with a slope of 1.68×10^{-2} GPa/μm with elongation of the NFBC. When the NFBC was stretched by 380 μm (corresponding to $F = 250$ μN), the stress reached 6.4 GPa.

Optics EXPRESS

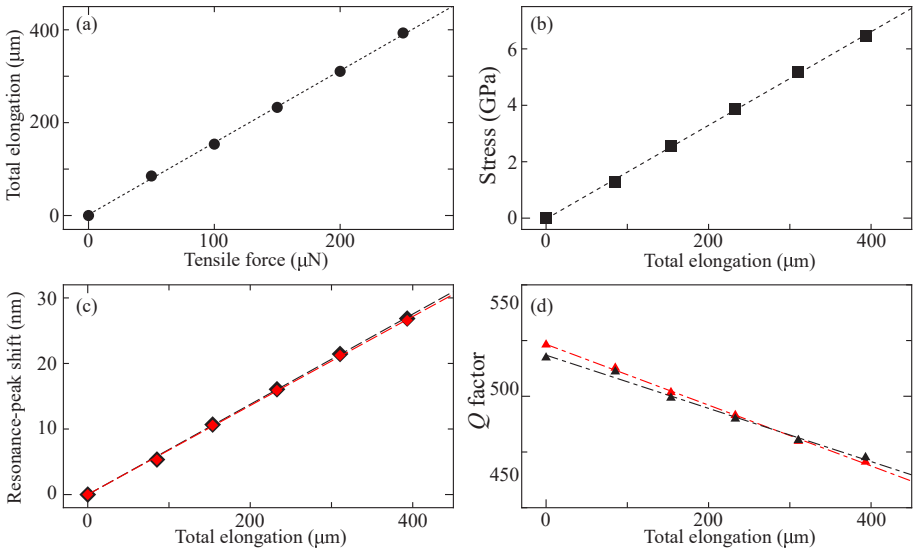

Fig. 4. (a) Dependence of calculated elongation on tensile force. (b) Dependence of stress at groove on elongation. (c) Dependence of resonance-peak shift on elongation. (d) Dependence of Q factor on elongation. The symbols and lines in these figures are the calculation results and the fitting results using a linear function, respectively. The black and red colors in (c) and (d) mean y-polarized mode and z-polarized mode, respectively.

We calculated the dependence of the resonance-peak shift on the change in the total elongation of the NFBC (tuning slope). Figure 4(c) shows the calculation results. The diamonds are the calculation results and the chained lines indicates the results of fitting using a linear function. The black and red colors mean y-polarized mode and z-polarized mode, respectively. The peak shifts for the y-polarized mode agreed with those of the z-polarized mode. The tuning slope for each polarization modes is 0.07 nm/μm. This slope almost agrees with the experimental results for the NFBC (0.05 nm/μm) [19].

We also calculated the dependence of the Q factor on the total elongation. Figure 4(d) shows the calculation results. The triangles are the calculation results and the dashed lines indicate the results of fitting using a linear function. The black and red colors are the y-polarized mode and z-polarized mode, respectively. The Q factor for each mode decreased with increasing elongation. When the NFBC was stretched by 380 μm, the Q factor for the y-polarized mode changed from 535 to 443, which is about 17%. On the other hand, the Q factor for the z-polarized mode changed from 546 to 441, which is about 19%. Although it is difficult to identify the cause of the degradation of Q factor, we conjecture that non-uniform deformation of the grating structure occurs due to the fact that the structure lacks the translational symmetry. If this is the case, it may be possible to pre-compensate the non-uniform deformation by creating a grating structure so that even periodicity is obtained at a given stretch. For the y-polarized mode, the Purcell factor slightly decreased from 5.3 to 4.9, which is about 7.5%. Therefore, we believe this slight reduction seems acceptable for the application as single photon sources.

From the above analyses, it is clear that the ultra-wide tunability of the NFBC was due to both the elongation of the grating period and the shrinkage of the diameter.

Finally, we discuss the estimated maximum resonance-peak shift when the NFBC is stretched. Here, we assume that σ_{rup} for a silica nanowire with a diameter of 300 nm is 10 GPa, as has been reported [37]. The elongation of the NFBC was calculated to be 595 μm from the fitting results in Fig. 4(b). Taking into account the tuning slope of 0.07 nm/μm assuming a linear stress-strain

Optics EXPRESS

relationship, the resonance peak could be shifted by 42 nm. Note that since σ_{rup} depends on cracks and hydroxyl (OH) groups on the surface of the fiber [37], reduction of these influences would be important for realizing this huge resonance-peak shift.

To further improve the tunability of the NFBC, a cavity structure that best reduces the stress concentration should be considered. In general, stress concentration occurs at notches with sharp angles and at the corners of angular grooves. For the shape of the groove on the surface of the nanofiber, large semicircular grooves and angular grooves with rounded corners are desirable from the viewpoint of stress relaxation. By introducing these structures on the nanofibers using nano-fabrication technology with high resolution [22,38], it would be possible to further improve the tunability of the nanofiber cavity.

5. Conclusions

The mechanism of the ultra-wide tunability of an NFBC was analyzed using 3D FEM and 3D FDTD optical simulations. When a tensile force of 200 μN was applied to the NFBC, a stress of 5.18 GPa was concentrated at the bottoms of the grooves in the grating. At the same time, the grating period was extended from 300 to 313.2 nm, while the diameter changed from 300 to 297.1 nm in the y-axis direction and from 300 to 298 nm in the z-axis direction. As a result, the wavelength of the resonance peak increased by 21.5 nm. The results of this analysis indicate that the ultra-wide tunability of the NFBC is due to both elongation of the grating period and the slight shrinking of the diameter. From the calculations of the stress at the groove, the resonance wavelength, and the Q factor for different total elongations, it was found that the dependence of the stress and the resonance wavelength was 1.68×10^{-2} GPa/μm and 0.07 nm/μm, respectively. Although the Q factor was slightly reduced under elongation, the decrease seemed acceptable for the application as single photon sources. Furthermore, we determined that the tuning range could be extended to 42 nm assuming a rupture strain of 10 GPa. Considering cavity structures with small stress concentrations, these simulation methods will be useful for realizing NFBCs with wider tuning ranges.

Funding. Japan Society for the Promotion of Science (19K03686, 21H04444, 22H01155, 26220712); Core Research for Evolutional Science and Technology (JPMJCR1674); The MEXT Quantum Leap Flagship Program (MEXT Q-LEAP) (JPMXS0118067634); Matsuo Foundation; Precursory Research for Embryonic Science and Technology (JPMJPR2257); Deutsche Forschungsgemeinschaft (390837967).

Acknowledgments. We gratefully acknowledge financial support in the form of Kakenhi Grants-in-Aid (Nos. 21H04444, 26220712, 22H01155, and 19K03686) from the Japan Society for the Promotion of Science (JSPS), the CREST program of the Japan Science and Technology Agency (JST) (JPMJCR1674), and the MEXT Quantum Leap Flagship Program (MEXT Q-LEAP) (JPMXS0118067634). H. T. acknowledges the support of the Matsuo Foundation and JST, PRESTO Grant Number JPMJPR2257, Japan. A. W. S. was supported by Deutsche Forschungsgemeinschaft (DFG, German Research Foundation) under Germany's Excellence Strategy - EXC-2123 Quantum Frontiers - 390837967.

Disclosures. The authors declare that there are no conflicts of interest related to this article.

Data availability. Data underlying the results presented in this paper are not publicly available at this time but may be obtained from the corresponding author (S. Takeuchi) upon reasonable request.

References

1. F. Vollmer, L. Yang, and S. Fainman, "Label-free detection with high-Q microcavities: A review of biosensing mechanisms for integrated devices," Nanophotonics **1**(3-4), 267–291 (2012).
2. H. Yokoyama, "Physics and device applications of optical microcavities," Science **256**(5053), 66–70 (1992).
3. T. J. Kippenberg and K. J. Vahala, "Cavity Opto-Mechanics," Opt. Express **15**(25), 17172–17205 (2007).
4. H. J. Kimble, "The quantum internet," Nature **453**(7198), 1023–1030 (2008).
5. H. Oka, H. F. Hofmann, S. Takeuchi, and K. Sasaki, "Effects of Decoherence on the Nonlinear Optical Phase Shift Obtained from a One-Dimensional Atom," Jpn. J. Appl. Phys. **43**(11A), 7495–7500 (2004).
6. S. Takeuchi, "Recent progress in single-photon and entangled-photon generation and applications," Jpn. J. Appl. Phys. **53**(3), 030101 (2014).
7. M. Pelton, C. Santori, J. Vučković, B. Zhang, G. S. Solomon, J. Plant, and Y. Yamamoto, "Efficient Source of Single Photons: A Single Quantum Dot in a Micropost," Phys. Rev. Lett. **89**(23), 233602 (2002).

Optics EXPRESS

8. Q. A. Turchette, C. J. Hood, W. Lange, H. Mabuchi, and H. J. Kimble, "Measurement of Conditional Phase Shifts for Quantum Logic," Phys. Rev. Lett. **75**(25), 4710–4713 (1995).
9. A. Chiba, H. Fujiwara, J. I. Hotta, S. Takeuchi, and K. Sasaki, "Resonant frequency control of a microspherical cavity by temperature adjustment," Jpn. J. Appl. Phys. **43**(9R), 6138–6141 (2004).
10. R. Henze, J. M. Ward, and O. Benson, "Temperature independent tuning of whispering gallery modes in a cryogenic environment," Opt. Express **21**(1), 675–680 (2013).
11. C. Singer, A. Goetz, A. S. Prasad, M. Becker, M. Rothhardt, and S. M. Skoff, "Thermal tuning of a fiber-integrated Fabry-Pérot cavity," Opt. Express **29**(18), 28778–28786 (2021).
12. K. N. Dinyari, R. J. Barbour, D. A. Golter, H. Wang, J. Pan, Y. Huo, K. Yamanaka, S. Sandhu, L. Scaccabarozzi, R. Timp, M. L. Povinelli, S. Fan, M. M. Fejer, J. S. Harris, D. Armani, B. Min, A. Martin, and K. J. Vahala, "Aligning microcavity resonances in silicon photonic-crystal slabs using laser-pumped thermal tuning," Appl. Phys. Lett. **92**(10), 103114 (2008).
13. J. Wang, K. P. Nayak, and J. Keloth, "Photothermal tuning and stabilization of a photonic crystal nanofiber cavity," Opt. Lett. **44**(16), 3996–3999 (2019).
14. D. Armani, B. Min, A. Martin, and K. J. Vahala, "Electrical thermo-optic tuning of ultrahigh-Q microtoroid resonators," Appl. Phys. Lett. **85**(22), 5439–5441 (2004).
15. S. Mosor, J. Hendrickson, B. C. Richards, J. Sweet, G. Khitrova, H. M. Gibbs, T. Yoshie, A. Scherer, O. B. Shchekin, and D. G. Deppe, "Scanning a photonic crystal slab nanocavity by condensation of xenon," Appl. Phys. Lett. **87**(14), 141105 (2005).
16. K. Srinivasan and O. Painter, "Optical fiber taper coupling and high-resolution wavelength tuning of microdisk resonators at cryogenic temperatures," Appl. Phys. Lett. **90**(3), 031114 (2007).
17. K. N. Dinyari, R. J. Barbour, D. A. Golter, and H. Wang, "Mechanical tuning of whispering gallery modes over a 05 THz tuning range with MHz resolution in a silica microsphere at cryogenic temperatures," Opt. Express **19**(19), 17966–17972 (2011).
18. K. P. Nayak, F. Le Kien, Y. Kawai, K. Hakuta, K. Nakajima, H. T. Miyazaki, and Y. Sugimoto, "Cavity formation on an optical nanofiber using focused ion beam milling technique," Opt. Express **19**(15), 14040–14050 (2011).
19. A. W. Schell, H. Takashima, S. Kamioka, Y. Oe, M. Fujiwara, O. Benson, and S. Takeuchi, "Highly Efficient Coupling of Nanolight Emitters to a Ultra-Wide Tunable Nanofibre Cavity," Sci. Rep. **5**(1), 9619 (2015).
20. W. Li, J. Du, V. G. Truong, and S. Nic Chormaic, "Optical nanofiber-based cavity induced by periodic air-nanohole arrays," Appl. Phys. Lett. **110**(25), 253102 (2017).
21. W. Li, J. Du, and S. Nic Chormaic, "Tailoring a nanofiber for enhanced photon emission and coupling efficiency from single quantum emitters," Opt. Lett. **43**(8), 1674–1677 (2018).
22. H. Takashima, A. Fukuda, H. Maruya, T. Tashima, A. W. Schell, and S. Takeuchi, "Fabrication of a nanofiber Bragg cavity with high quality factor using a focused helium ion beam," Opt. Express **27**(5), 6792–6800 (2019).
23. T. Tashima, H. Takashima, A. W. Schell, T. T. Tran, I. Aharonovich, and S. Takeuchi, "Hybrid device of hexagonal boron nitride nanoflakes with defect centres and a nano-fibre Bragg cavity," Sci. Rep. **12**(1), 96 (2022).
24. F. L. Kien, J. Liang, K. Hakuta, and V. Balykin, "Field intensity distributions and polarization orientations in a vacuum-clad subwavelength-diameter optical fiber," Opt. Commun. **242**(4-6), 445–455 (2004).
25. L. Tong, R. R. Gattass, J. B. Ashcom, S. He, J. Lou, M. Shen, I. Maxwell, and E. Mazur, "Subwavelength-diameter silica wires for low-loss optical wave guiding," Nature **426**(6968), 816–819 (2003).
26. F. Le Kien, S. Dutta Gupta, V. I. Balykin, and K. Hakuta, "Spontaneous emission of a cesium atom near a nanofiber: Efficient coupling of light to guided modes," Phys. Rev. A **72**(3), 032509 (2005).
27. M. Almokhtar, M. Fujiwara, H. Takashima, and S. Takeuchi, "Numerical simulations of nanodiamond nitrogen-vacancy centers coupled with tapered optical fibers as hybrid quantum nanophotonic devices," Opt. Express **22**(17), 20045–20059 (2014).
28. M. Fujiwara, K. Toubaru, T. Noda, H.-Q. Zhao, and S. Takeuchi, "Highly Efficient Coupling of Photons from Nanoemitters into Single-Mode Optical Fibers," Nano Lett. **11**(10), 4362–4365 (2011).
29. R. Yalla, F. Le Kien, M. Morinaga, and K. Hakuta, "Efficient Channeling of Fluorescence Photons from Single Quantum Dots into Guided Modes of Optical Nanofiber," Phys. Rev. Lett. **109**(6), 063602 (2012).
30. A. Stiebeiner, O. Rehband, R. Garcia-Fernandez, and A. Rauschenbeutel, "Ultra-sensitive fluorescence spectroscopy of isolated surface-adsorbed molecules using an optical nanofiber," Opt. Express **17**(24), 21704–21711 (2009).
31. T. Schröder, M. Fujiwara, T. Noda, H.-Q. Zhao, O. Benson, and S. Takeuchi, "A nanodiamond-tapered fiber system with high single-mode coupling efficiency," Opt. Express **20**(10), 10490–10497 (2012).
32. L. Liebermeister, F. Petersen, A. v. Münchow, D. Burchardt, J. Hermelbracht, T. Tashima, A. W. Schell, O. Benson, T. Meinhardt, A. Krueger, A. Stiebeiner, A. Rauschenbeutel, H. Weinfurter, and M. Weber, "Tapered fiber coupling of single photons emitted by a deterministically positioned single nitrogen vacancy center," Appl. Phys. Lett. **104**(3), 031101 (2014).
33. K. P. Nayak, P. Zhang, and K. Hakuta, "Optical nanofiber-based photonic crystal cavity," Opt. Lett. **39**(2), 232–235 (2014).
34. J. Keloth, K. P. Nayak, and K. Hakuta, "Fabrication of a centimeter-long cavity on a nanofiber for cavity quantum electrodynamics," Opt. Lett. **42**(5), 1003–1006 (2017).
35. S. Holleis, T. Hoinkes, C. Wuttke, P. Schneeweiss, and A. Rauschenbeutel, "Experimental stress-strain analysis of tapered silica optical fibers with nanofiber waist," Appl. Phys. Lett. **104**(16), 163109 (2014).

Optics EXPRESS

36. H. Takashima, M. Fujiwara, A. W. Schell, and S. Takeuchi, "Detailed numerical analysis of photon emission from a single light emitter coupled with a nanofiber Bragg cavity," Opt. Express **24**(13), 15050–15058 (2016).
37. G. Brambilla and D. N. Payne, "The Ultimate Strength of Glass Silica Nanowires," Nano Lett. **9**(2), 831–835 (2009).
38. B. W. Ward, J. A. Notte, and N. P. Economou, "Helium ion microscope: A new tool for nanoscale microscopy and metrology," J. Vac. Sci. Technol., B: Microelectron. Nanometer Struct.–Process., Meas., Phenom. **24**(6), 2871–2874 (2006).